Mechanochemical synthesis of structurally well-defined graphitic phosphorus-linked carbon nitride (g-PCN) with water splitting activity

Blaine G. Fiss,[a] † Georgia Douglas,[a] † Michael Ferguson,[a] Jorge Becerra,[b] Jesus Valdez,[c] Trong-On Do,[b] Tomislav Friščić,*[a] Audrey Moores*[a,d]*

a. Centre in Green Chemistry and Catalysis, Department of Chemistry, McGill University, 801 Sherbrooke Street West, Montréal, Québec, Canada

b. Department of Chemical Engineering, Laval University, Québec City, Québec, Canada

c. Facility for Electron Microscopy Research (FEMR), McGill University Montréal, Québec, Canada

d. Department of Materials Engineering, McGill University, 3610 University Street, Montréal, Québec, Canada

corresponding authors: Tomislav.friscic@mcgill.ca; audrey.moores@mcgill.ca

KEYWORDS: Mechanochemistry, Carbon nitride, Phosphorus, Density Functional Theory, Hydrogen evolution

Dedicated to the memory of Prof. Pascal Le Floch

ABSTRACT Heteroatom-doped carbon nitride (CN) materials have shown much potential as metal-free photocatalysts for water splitting. Graphitic phosphorus-linked triazine network (g-PCN) materials are a unique class within this family of materials, but remain difficult to access due to long reaction times annealing at temperatures above 500 °C and often afford ill-understood structures. Here, we reveal a milder, lower temperature approach for the synthesis of catalytically active g-PCN materials through combining a room-temperature mechanochemical reaction of sodium phosphide and cyanuric chloride with brief (1 hour) annealing of the milled material at 300 °C. This rapid, low temperature procedure yields ordered g-PCN catalysts whose layered structure was determined through a combination of magic-angle spinning nuclear magnetic resonance (MAS NMR), X-ray photoelectron spectroscopy (XPS), powder X-ray diffraction (PXRD) and transmission electron microscopy (TEM). An excellent level of accuracy to simulated ^{31}P MAS NMR signals and PXRD patterns were obtained for the structure of the synthesized layered phosphorus-linked triazine networks following dispersion-corrected density functional theory (DFT). The mechanochemically-generated g-PCN is a highly effective photocatalyst for the hydrogen evolution reaction, producing 122 μmol H_2 h^{-1} g^{-1} under broad spectrum irradiation.

Introduction

Over the last decade, photocatalytic water splitting has attracted much attention as a potentially sustainable route to hydrogen gas production. The scaling-up of the water splitting process is urgently needed as today, hydrogen gas is primarily obtained through the steam reforming of natural gas, an energy-intensive process producing carbon monoxide and dioxide as by-products.[1] Recent improvements in water splitting catalysis have led to the development of new cocatalysts and photoactive supports to further increase the rate of reaction. Much of this work has focused on the design of new earth-abundant cocatalysts such as metal oxides,[2,3] hydroxides,[4,5] sulfides,[6,7]

phosphates[8] and phosphides.[9-11] In terms of photocatalytic supports, graphitic carbon nitride (g-C_3N_4) has been one of the most promising candidates, due to its potential as a metal-free, heterogeneous photocatalyst, which is also readily modifiable towards different morphologies and dopants.[12,13] While g-C_3N_4 has attracted interest as a metal-free semiconductor, challenges remain related to the understanding of its exact structure,[14] photophysical properties,[15,16] and its relatively wide band gap as a semiconductor[17] restricts its use as a photocatalyst for broad spectrum water splitting. Photocatalytic activity of g-C_3N_4 can be enhanced by doping with heteroatoms, such as boron, oxygen,[18,19] sulfur[20,21] or phosphorus,[21-23] in order to tune its band gap and improve exciton generation.[13] The Antonietti group has detailed the successful application of g-C_3N_4 for hydrogen production from water under visible light,[24] while further developments explored the inclusion of phosphorus in this structure to afford phosphorus-doped graphitic carbon nitrides or carbon phosphanitride materials,[25] applicable as photocatalysts for a range of reactions, including the hydrogen evolution reaction (HER),[26,27] oxygen evolution reaction (OER),[28,29] and diverse photodegradation reactions.[30-32]

Typical syntheses of phosphorus-containing graphitic carbon nitride rely on the hydrothermal carbonization (HTC) of triazine-containing starting material, such as melamine or cyanuric chloride as carbon and nitrogen precursors, and a phosphorus source, forming various polymeric carbon phosphanitrides. Alternatively, small molecular precursors containing all three elements, such as $P(CN)_3$, have been thermally treated to afford extended C_3N_3P materials, as reported by Epshteyn, Strobel and coworkers (Scheme 1b).[33,34] Additionally, a microwave synthesis of phosphorus-doped graphitic carbon nitride nanosheets for electrochemiluminescence applications has been reported by Wang and coworkers in 2020 (Scheme 1c).[35] However, these syntheses typically employ high-temperature furnace techniques, annealing for relatively long periods of

time, or in the case of microwave synthesis, rely on the use of bulk solvent to disperse the starting materials.

Recently, mechanochemistry has gained popularity as an approach for cleaner, solvent-free synthesis, typically based on ball milling for batch processes or twin-screw extrusion (TSE)[36-39] as a means of continuous processing, with a range of demonstrated applications in materials synthesis and design.[40] Mechanochemistry has been applied with much success towards various organic[41-44] and inorganic[45-49] reactions, synthesis of advanced materials such as metal-organic frameworks (MOFs),[50-52] polymers,[53-56] cocrystals,[57,58] and nanoparticle-based materials.[59-64]

The synthesis of heteroatom-doped carbon nitrides, especially when incorporating phosphorus atoms, have relied on the use of non-conventional phosphorus sources, allowing for more atom-economical and low temperature syntheses. Common reagents include pentafluorophosphate-containing ionic liquids,[25] red phosphorus,[65] phytic acid,[66] ammonium hypophosphite and phosphates,[35,67] as well as $P(CN)_3$.[33,34] Sodium phosphide has shown potential in low-temperature access to unique low-valent phosphorus compounds,[68] as well as access to metal phosphide nanoparticles.[69] Consequently, we hypothesized that ball-milling of sodium phosphide (Na_3P) together with cyanuric chloride as a commercially available triazine linker would provide room-temperature access to layered, phosphorus-linked triazine networks through a low temperature mechanochemical metathesis[70] reaction. (Scheme 1d).

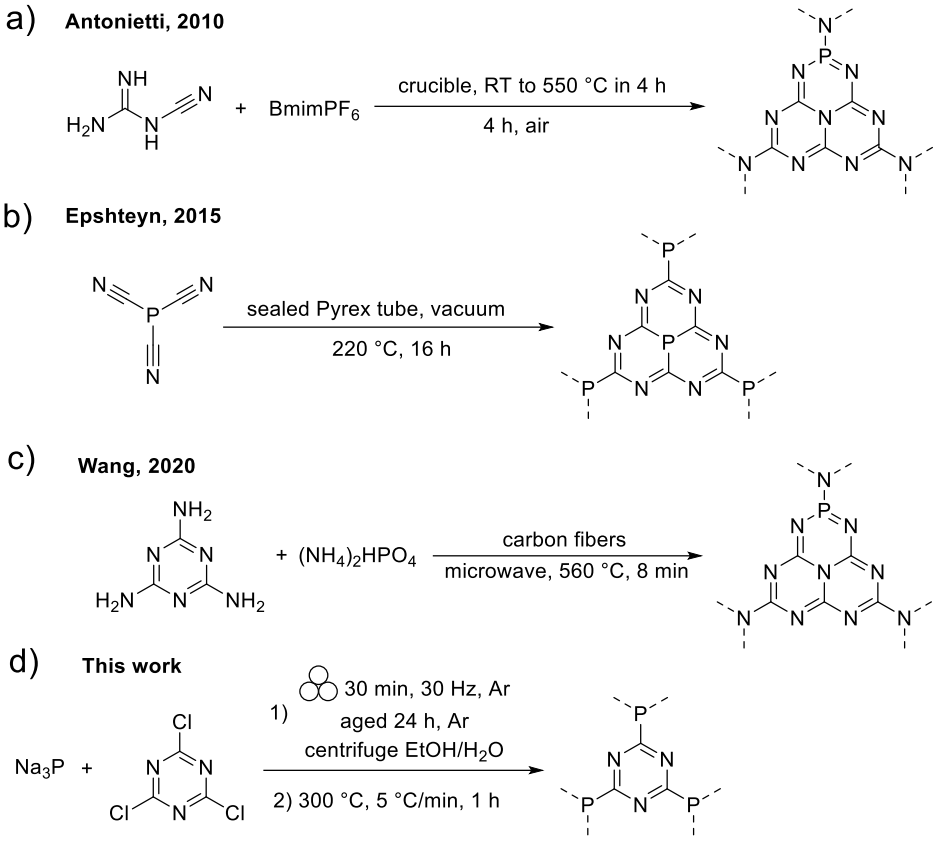

Scheme 1. Key examples of phosphanitride and phosphorus-containing graphitic carbon nitride presented by a) Antonietti b) Epshteyn c) Wang and d) the presented work.

Several recent reports have described the elegant mechanosynthesis of heteroatom-bridged carbon nitride materials, including those on doped porous covalent-organic frameworks (COFs). For example, Casco and coworkers showed the mechanochemical synthesis of N-doped porous carbons through a mechanically-induced self-sustaining reaction (MSR)[71-73] between cyanuric chloride and CaC_2 with milling times as short as 5 min. The resultant material contained up to 16 wt% of nitrogen and formed $CaCl_2$ as a side product.[74] Cyanuric chloride was also used a triazine unit, alongside a variety of aromatic monomers, and $AlCl_3$ as an activating unit, in the mechanochemical Friedel-Crafts alkylation to synthesize porous covalent triazine frameworks.[75]

In contrast to significant interest in phosphorus-linked carbon nitride materials, so far, there has been very limited experimental work corroborating their structures.

Here, we demonstrate how mechanochemistry enables a simple, mild route for the synthesis of novel carbon phosphanitride materials by milling of cyanuric chloride as a source of the triazine unit with sodium phosphide (Na_3P) as a reactive solid phosphorus source. The use of mechanochemical milling enabled the synthesis of a carbon phosphanitride under significantly milder conditions than previously reported, by combining a brief mechanochemical step with room-temperature ageing and a brief (1 hour) exposure to 300 ºC. By combining a range of solid-state analytical techniques with dispersion-corrected density-functional theory (DFT) modelling we were able to provide unambiguous confirmation of its structure. In combination with Pt nanoparticles, the resulting carbon phosphanitride material exhibits high activity for water splitting, presenting a unique example of a carbon phosphanitride that can be obtained under mild conditions, is structurally well-characterized, and provides functional behavior as a photoactive support.

Results and Discussion

The presented mechanosynthesis of phosphorus-linked triazine networks involved ball milling of equimolar quantities of Na_3P with cyanuric chloride under an argon atmosphere. In a typical experiment, the reactants were added to a zirconia milling apparatus along with two zirconia milling balls of 7 mm diameter, and the reaction mixture was milled for 30 minutes at a frequency of 30 Hz, followed by aging for 24 hours under an argon atmosphere for in a glovebox. Our previous work has demonstrated the ability to obtain well-defined nanostructured materials simply by brief mechanical activation through ball milling, followed by ageing at room temperature.[76-78] After aging, the jars were opened in air, their content taken up into a 3:1 v/v mixture of EtOH and

deionized (DI) water, and the system separated by centrifugation, before drying *in vacuuo* at 50 °C for 12 h prior to analysis. Attempts to obtain the same material by milling for shorter times or using a single zirconia ball of 10 mm diameter led to incomplete transformation, as evident by violent hydrolysis of unreacted Na_3P upon washing of the final product. The effect of a post-synthetic annealing step was also investigated. The as-made carbon phosphanitride (g-PCN) material was placed into an alumina crucible, wrapped loosely in aluminum foil and heated in a tube furnace under a flow of argon gas for 1 h at either 200 or 300 °C, producing samples denoted as g-PCN200 and g-PCN300, respectively. As a phosphorus-free reference, graphitic carbon nitride (g-C_3N_4) was produced through a previously reported furnace-based method of thermally annealing melamine at 525 °C for 4 h.[79]

The crystallinity of the samples before annealing and after thermal treatment was evaluated by powder X-ray diffraction (PXRD). For the non-annealed samples, two broad Bragg reflections are seen at approximately $2\theta = 15°$ and 26° (Figure 1, teal). The measured crystallinity index (CrI) for g-PCN before annealing was determined to be 21%, showing a largely amorphous material being formed after the milling and aging process. Upon annealing at 200 °C, negligible change was noted in the PXRD pattern (Figure 1, blue). The most significant change was seen for the g-PCN300 sample, where annealing led to an increase in CrI to 33%, as well as the appearance of novel X-ray reflections (Figure 1, purple), suggesting an increase in the ordering of the graphitic structure of the material.

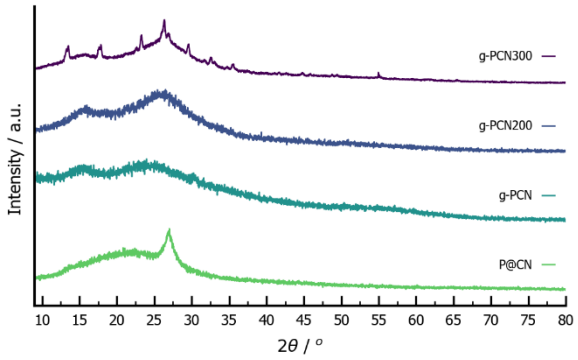

Figure 1. PXRD patterns of phosphorus-linked g-C_3N_4, g-PCN, g-PCN200 and g-PCN300.

The formation of a phosphorus-linked triazine was verified by X-ray photoelectron spectroscopy (XPS), solid-state magic angle spinning ^{31}P NMR (MAS NMR), and Fourier-transform infrared attenuated total reflectance (FTIR-ATR) spectroscopy, which also permitted the quantification and speciation of phosphorus loading.

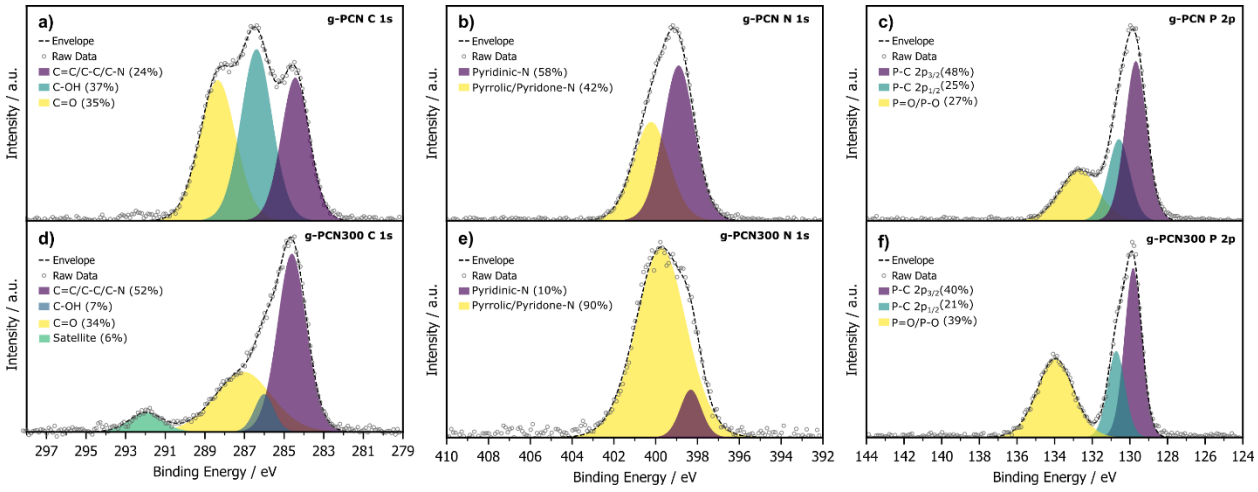

Figure 2. Comparison of XPS scans for C 1s b) N 1s and c) P 2p scans of g-PCN and d) C 1s e) N 1s and f) P 2p scans of g-PCN300.

The XPS C 1s focused scan of the g-PCN material showed three maxima at 248.4, 286.5, and 288.6 eV, confirming the presence of C=N, C-OH, and C=O species, respectively (Figure 2a).[80] The signal corresponding to C=N bonds confirmed the retention of the triazine linker following

milling with Na_3P and aging. The presence of the C-OH bonds suggests that upon centrifuging the g-PCN for a total of 15 min using a 3:1 EtOH:H_2O (v/v) mixture, terminal chloride units on the pendant triazine fragments are hydrolyzed to form hydroxyl moieties. Similarly, the presence of carbonyl absorption bands at ~1600 cm^{-1}, which is seen in FTIR-ATR data (Figure S1), suggests the partial hydrolysis of the triazine ring to give amide functionalities. XPS N 1s focused scans (Figure 2b) further validate this hypothesis as two deconvoluted maxima at 398.9 and 399.9 eV are observed, which correspond to pyridinic and pyridine species for nitrogen. This suggests that unreacted terminal chlorides were still present on the edges of the material after the reaction and have hydrolyzed during work up. Focused scans of the P 2p signal showed a doublet consisting of two maxima centred at 129.8 eV, highlighting P-C bond character as well as a broader maximum centred at 133.2 eV, which highlights both the formation of bridging phosphorus centers between triazine rings, as well as their partial oxidation, which was quantified at 48% upon deconvolution and integration of the XPS data (Figure 2c). Comparing to furnace-made phosphorus-doped carbon nitride (P@CN),[81] C 1s focused scans in XPS showed two signals, at 284.7 eV and 287.9 eV, corresponding to C=N/C-N and C=O bonds respectively (Figure S3a). N 1s focused scans showed two major maxima at 397.4 eV and 398.7 eV, consistent with a majority of nitrogen being in the form of pyrrolic species, compared to pyridine-type nitrogen species that were observed in the furnace-made P@CN (Figure S3b). The P 2p scan showed only a doublet for P-O/P=O type bonds, centered at 133.4 eV (Figure S3c). Finally, the O 1s scan indicated the presence of two species, similar to g-PCN, at 531.1 eV and 533.0 eV, showing 39% -OH character, with 61% of species coming from an O^{2-} species (Figure S3d).

Due to low crystallinity of the mechanochemically prepared samples, a subsequent annealing step under an argon atmosphere was conducted for 1 hour at either 200 or 300 °C.

Thermogravimetric analysis (TGA) confirmed that exposure to such temperatures does not lead to a significant mass upon heating in a nitrogen atmosphere (Figure S2). After annealing at 200 °C for 1 h under argon, the C 1s XPS focused scans of the resulting phosphorus-linked triazine network (g-PCN200) showed three signals as before annealing, at 284.6, 287.4 and 285.9 eV. These signals correspond to bonds of the C=N/C-N, C-OH and C=O character, respectively (Figure S4a). Of note is the decrease in the percentage of C-OH character after annealing, from 37% to 10% while the carbonyl character increased from 35% to 59%. The N 1s scans showed a shift in the majority signal to favor pyrrolic N character on its surface up to 73% following the anneal (Figure S4b). The P 2p focused scans also showed an increase of the P-O/P=O character upon annealing at 200 °C, from 27 to 64% (Figure S4c). In contrast, the O 1s scans remained largely unchanged for the sample, favoring species of the O^{2-} type (evaluated at 64% abundance) for g-PCN200 (Figure S4d).

Upon annealing at 300 °C for 1 h, the deconvolution of the C 1s scans revealed maxima at 284.7, 286.3, 287.6, and 292.0 eV (Figure 1d). The respective ratios of these signals demonstrate a decrease in the relative quantity of hydroxyl C-OH character, implying a loss of terminal hydroxyl groups moieties and an increase in the relative abundance of graphitic nitride character. The consistency of the amount of carbonyl signal shows that partially hydrolyzed triazine units are still present, even after annealing. This trend is further supported by observing the ratio of pyridinic and pyridine-N character (Figure 1e), which showed a 90% relative content of triazines with hydrolyzed hydroxyl groups. The P 2p focused scan (Figure 1f) showed a small increase in the degree of oxidation from 27 to 39%, however the sample was still predominantly P-C in character, supporting the maintained integrity of the material after annealing.

Structural information for the phosphorus-linked triazine networks was also acquired through FTIR-ATR spectroscopy. Compared to g-C_3N_4, the mechanochemically synthesized g-PCN materials similarly show C-N heterocycle stretches in the 1200-1600 cm^{-1} range (Figure S1).[82] For the sample annealed at 300 °C, g-PCN300, a band present at 1615 cm^{-1} can be attributed to a C=N stretch, and the bands at ~810 cm^{-1} can be matched to the vibrational fingerprint of the triazine unit,[83] further suggesting the graphitic structure was preserved after both ball milling and annealing. While the absorption band at 534 cm^{-1} could also be associated with P-C bond character,[33] other phosphorus-related stretches may overlap with the strong C-N vibrations.

Scanning transmission electron microscopy (STEM) analysis using a high angle annular dark field detector (HAADF) revealed that g-PCN200 and g-PCN300 featured a layered structure. This is remarkable since these types of properties are seen in g-C_3N_4 typically when annealed at temperatures above 500 °C (Figure 3a). [84]

We obtained the relative thickness of g-PCN, g-PCN200 and g-PCN300 using electron energy loss spectroscopy (EELS). Relative thickness is the mean number of scattering events per incident electron and can be obtained in the low-loss region of an EELS spectrum. HAADF relative intensity also validated these results.[85,86] In our specimens, we observed that the relative thickness increases from pristine g-C_3N_4 at 0.34 to 0.90 for g-PCN, and relative thicknesses of 0.73 and 0.66 for g-PCN200 and g-PCN300, respectively, showing an inversed relationship of relative thickness to annealing temperature. This follows similarly reported trends, wherein graphitic carbon nitride films show a similar reduction in thickness as annealing temperature is increased from 150 °C up to 500 °C.[87]

The EELS analysis of g-PCN (prior to any annealing) showed an even distribution of carbon, nitrogen, and oxygen throughout the material, while phosphorus appeared localized to specific

regions (Figure 3b). A similar localization of phosphorus was also seen on g-PCN200 (Figure 3c). However, upon increasing the annealing temperature to 300 °C, the distribution of phosphorus becomes more uniform. This distribution of phosphorus correlates with an increase in the presence of PXRD signals matching the predicted layered structure (Figure 3).

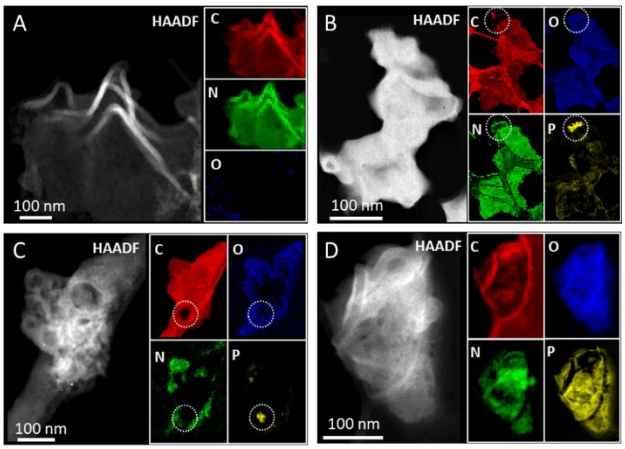

Figure 3. STEM-HAADF images (left) and EELS maps (right) for the characteristic elements presented on graphitic carbon networks. a) g-C_3N_4 network without any thermal treatment or phosphorus bridges is compared with b) g-PCN (no annealing), c) g-PCN200 (annealing at 200 °C) and d) g-PCN300 (annealing at 300 °C) Dotted white circles denote localized regions of high phosphorus density.

To better understand the photochemical properties of the mechanochemically-synthesized phosphorus-linked triazine networks, the samples were characterized by ultraviolet-visible diffuse reflectance spectroscopy (UV-DRS) and photoluminescence (PL) measurements. Pristine g-C_3N_4 showed a typical semiconductor-like absorption maximum centered around 400 nm, originating from the charge transfer response of g-C_3N_4 from the valence band (VB) populated by N 2p orbitals to the conduction band (CB) formed by C 2p orbitals.[30,31,33] For the mechanochemically-synthesized phosphorus-linked triazine networks, a red shift of the absorption band is seen in comparison to pristine g-C_3N_4. g-PCN samples, made by milling for 30 min and aging for 24 h

showed a red-shifted maximum at 518 nm, suggesting a decrease in the band gap energy compared to g-C_3N_4. After annealing of the g-PCN material at either 200 °C or 300 °C–g-PCN200 and g-PCN300, the absorption band is further broadened across the visible light range, with a maximum absorbance peak around 530 nm (Figure 4a).

In PL measurements a strong, broad signal is observed for pristine g-C_3N_4, and a much weaker signal for all g-PCN samples, with a minor increase in intensity seen as a function of annealing temperature (Figure 4b). These results infer that the generated exciton in the phosphorus-linked samples is recombining at a slower rate than g-C_3N_4, with bridging nitrogen, resulting in increased excited state lifetimes (Figure 4c). For pristine g-C_3N_4, a τ value of 4.2 μs was noted, which gradually increased to 4.7, 41, and 39 μs for g-PCN, g-PCN200 and g-PCN300, respectively. This increase by an order of magnitude upon addition of phosphorus linkages and subsequent annealing suggests improved stability of the charged species, without the need for an additional cocatalyst.[22,88]

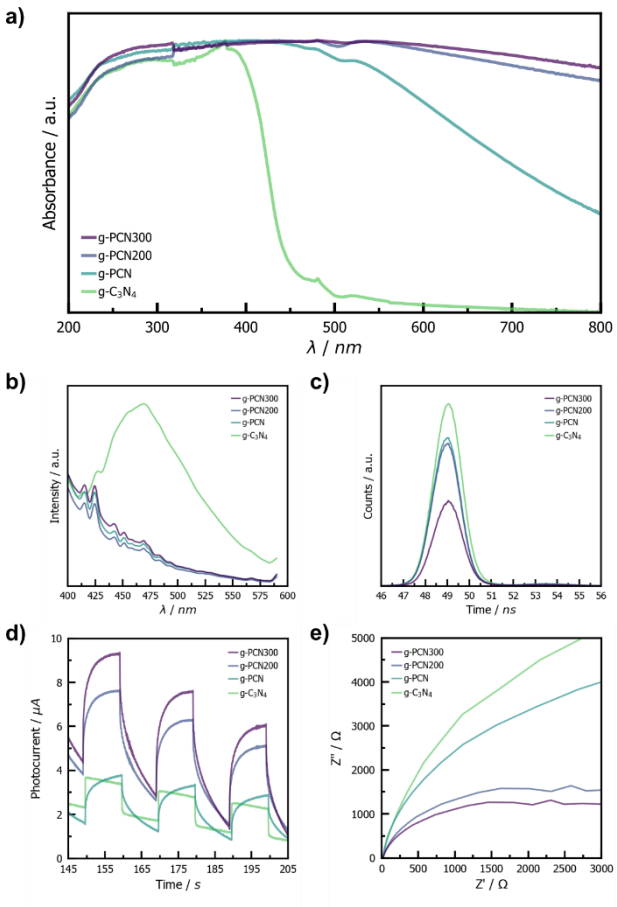

Figure 4. a) UV-Vis DRS b) photoluminescence b) lifetime c) photocurrent and e) Nyquist plots of g-C_3N_4 (green), g-PCN (teal), g-PCN200 (blue) and g-PCN300 (purple).

The temporal photocurrent of g-PCN, g-PCN200, and g-PCN300 was then investigated to verify that the introduction of phosphorus into the triazine network improved the charge transport upon irradiation. The g-C_3N_4 material, which is typically nitrogen-linked, showed a maximum photocurrent of 1 μA (Figure 4c, green traces), g-PCN prior to any annealing featured a similar photocurrent performance (Figure 4c, teal trace). Upon annealing at 200 °C and 300 °C, the photocurrent increases to a maximum of 4 μA and 5 μA respectively (Figure 4c, blue and purple traces). Furthermore, the electrochemical impedance spectroscopy (EIS) (Figure 4e) showed a decrease in the impedance for the materials where g-C_3N_4 > g-PCN > g-PCN200 > g-PCN300.

This implies that incorporating phosphorus as the linking atom led to an enhancement of the photoelectrochemical properties. A lower arc radius, implying better charge transer,[89,90] was noted for the g-PCN series of materials compared to the native g-C_3N_4. These enhancements were furthered by annealing g-PCN at 200 and 300 °C. This effect could be seen in the improvement of the photocatalytic activity for the g-PCN series compared to g-C_3N_4. Finally, band structure was studied by Mott-Schottky technique (Figure S4, see ESI for details). All phosphorus-containing samples exhibited a positive slope indicating an *n*-type semiconductor, characteristic of graphitic carbon nitride materials.[91,92] The conduction band of all as-prepared samples was determined from the *x*-intercept value, derived from the tangent line of the slope on the Mott Schottky plot. Accordingly, the estimated value for g-C_3N_4 was ~-1.10 V Ag/AgCl which corresponds to previous literature reports.[69, 93] For the nanocomposites it was observed a more negative band (-1.30, -1.40 and -1.25 V for g-PCN, g-PCN200 and g-PCN300, respectively). Considering the broad visible light absorption of the nanocomposites and the estimated values from Mott-Schottky, it could be inferred that synthesized materials are suitable for HER due to their band positions, as it is more negative than H_2 standard reduction potential, 0 V vs NHE at pH 7.[89,92,94]

We then turned to ^{31}P MAS NMR techniques in order to gain more insights into the chemical structure of the synthesized materials, as reported by others. [25,33,82] The spectrum of g-PCN (Figure S5a) featured mostly a broad and noisy band centered on δ_{P1} = 4.00 ppm with a broad shoulder at δ_{P2} = 26.65 ppm , while g-PCN200 (Figure S5b) had several resonances in a more downfield region at δ_{P1} = 0.84 ppm, δ_{P2} = -9.47 ppm and δ_{P3} = – 20.96 ppm. The PCN300 material exhibited the most easily interpreted spectrum with two peaks at δ_{P1} = -12.8. ppm and δ_{P2} = -24.7 ppm. This trend indicates that annealing results in an overall reduction of the phosphorus species inside the materials. This sharp resonance in the case of g-PCN300 is unprecedented for triazine-based,

phosphorus-linked carbon nitrides, as often broad resonances are seen even upon materials treated at high temperature and pressure.[34]

Next, we employed computational methods were employed to determine the species responsible for the individual signals found in the deconvoluted MAS NMR spectra. Gaussian 16[95] was used to optimize the structure and calculate the ^{31}P chemical shielding tensors for a variety of phosphorus-containing molecules serving as models in this context. These molecules were chosen to represent various stages of oligomerization of triazine rings bridged by phosphorus, III or V, and considered with either chloride or hydroxy functionalities (Chart S1). They were treated as isolated molecules in the gas phase and were described by an atom-centered basis set (6-311G). The analysis of the trends in chemical shifts of this family of molecules confirms that likely phosphorus containing molecules formed in this reaction are being reduced upon annealing. Also, despite the cleanliness of the recorded spectra, it was difficult to attribute unambiguously the peaks to one single computed structure, as eight of them fell in the $10 < \delta < -30$ ppm region (Table S1). To account for the pure product of the reaction, a perfectly repeating unit of g-PCN we employed periodic DFT calculations. The ^{31}P chemical shifts for bulk g-PCN were calculated using the periodic plane-wave DFT code CASTEP, v20.11,[96] following the work of Wang *et al.*,[34] whereby the bridging nitrogen atoms in the experimentally resolved structure of g-C_3N_4, reported by Algara-Siller *et al,*[97] were replaced with phosphorus (see details in Supplementary Information). Two unique phosphorus environments were seen in the DFT calculated structure of g-PCN. The environment termed P1 was calculated to have empty space above and below it, while the environment P2 is centered between triazine rings both above and below it (Figure 5, insert). Importantly, in this work we obtained a planar geometry from full structural and cell optimizations, which is different from the previously observed buckling of the g-PCN sheets.[34] Two chemical

shifts were obtained for the structure, δ_{P1} = -11.83 ppm and δ_{P2} = -23.47 ppm and correspond to the two different environments experienced by phosphorus atoms in the optimized structure. These numbers are in excellent agreement with the experimental data for g-PCN200 and g-PCN300. (Figure 5a, also SI Figure S5b,)

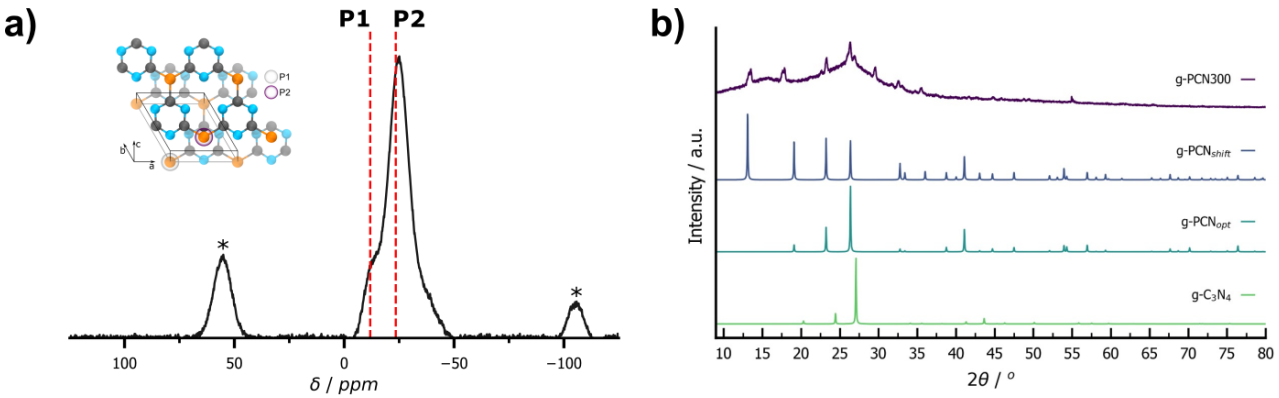

Figure 5. ^{31}P MAS NMR at 13 kHz of g-PCN300. Red lines denote shifts calculated using CASTEP-optimized structure (insert); b) From the bottom up: Simulated PXRD patterns of the g-C_3N_4 structure from Algara-Siller *et al.*[97] (TGCN); g-PCN$_{opt}$; g-PCNshift and g-PCN300. The asterisks denote spinning sidebands

Given the agreement between the calculated and experiment data for the optimized structure, we revisited the PXRD pattern of g-PCN300, which features sharp, distinct reflections over an amorphous background (Figure 5b, purple). The CASTEP simulated pattern for the optimized structure (Figure 5b, teal) exhibits X-ray reflections at 13.5 °, 23.3 °, 26.3 °, and 32.6 ° *2θ*, in good agreement with the experimental pattern for g-PCN300. We further improved on this agreement applying a translational distortion of 1% along the a-axis of the upper plane of the optimized structure (more positive in the c-axis). This provided more matching reflections at 23.3 °, 26.3 °, and 32.6 ° *2θ* (Figure 5b, blue). We also compared the pattern for g-PCN300 with the simulated pattern of the experimentally derived g-C_3N_4 structure from Algara-Siller and coworkers (Figure

5b, green), which revealed to be close, yet not matching, as expected from a non-phosphorus-containing structure with a similar reflection at a *2θ* of 26.9 °.

As has been previously highlighted, both by our group[69] as well as other researchers,[76,98,99] the use of sustainability metrics is paramount in demonstrating the benefit in energy-waste reduction that mechanochemical techniques have over the traditionally used high-temperature solid-state techniques often employed for layer carbon nitride based materials. Our group had previously shown that comparing the energy demand of a Retsch MM400 vibrational mill in comparison to tube furnace and solution-based routes to nickel phosphide nanoparticles[69] can also be employed in the present study (Table 1).

Table 1. Comparison of energy usage metrics for traditionally used annealing method, to the hybrid milling-aging-annealing method.

Method	Milling and Aging Time / h	Annealing / Temp, Time	Energy draw / $kWhg^{-1}$
Furnace	-	550 °C, 4 h	1.87
Ball milling	0.5, 24	-	0.19
Ball milling	0.5, 24	200 °C, 1 h	0.75
Ball milling	0.5, 24	300 °C, 1 h	1.07

A furnace-based synthesis of g-C_3N_4 conducted on a 2 g scale used 1.87 $kWhg^{-1}$ after 4 h, while the presented work, at only a 250 mg scale was shown to use only 1.07 $kWhg^{-1}$, combining both for the energy draw during the milling step and after annealing in a tube furnace at 300 °C for 1 h. Even before annealing, the mechanochemical formation of the g-PCN network shows an energy draw value 10 times lower than that of the g-C_3N_4.

The catalytic behaviour towards the hydrogen evolution reaction was optimized for a variety of reaction times, platinum cocatalyst loadings and total composite catalyst used. Initial studies

showed an increase in catalytic activity of g-PCN compared to g-C_3N_4. However, despite the increase in exciton lifetime and improved photocurrent upon annealing to obtain g-PCN200 and g-PCN300, catalytic activity was shown to decrease (Figure 6a).

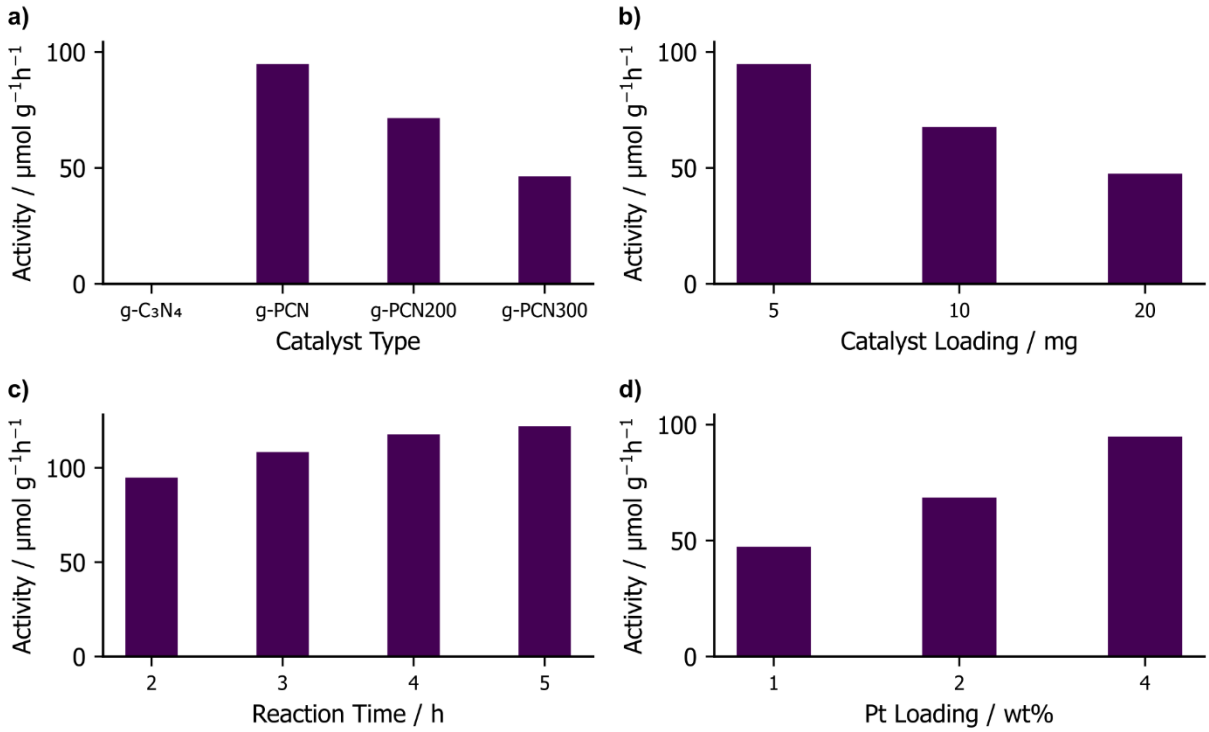

Figure 6. a) Catalytic activity of g-C3N4, g-PCN, g-PCN200 and g-PCN300 ,b) effect of mass loading of g-PCN, c) reaction time and d) loading of Pt cocatlyst on catalytic activity for 1 wt%, 2 wt% and 4 wt% of Pt.

Increasing the composite catalyst loading in the reaction also led to a decrease in catalytic activity, producing 68 µmol H_2 h^{-1} g^{-1} when using 10 mg and 47 µmol H_2 h^{-1} g^{-1} when using a total of 20 mg of composite catalyst (Figure 6b). This effect could be related to the haze created by the high amount (oversaturated) of dispersed photocatalyst blocking the light in the reaction medium. In parallel, it was also shown that 4 hours reaction times were the most efficient (Figure 6c) and that

a cocatalyst loading of 4 wt% Pt produced rates upwards of ca. 122 µmol H_2 h^{-1} g^{-1} (Figure 6d). The loss in catalytic activity with increasing annealing temperature led to investigating the effect of milling times, annealing temperature and further milling treatment following isolation. g-C_3N_4 made through a conventional tube furnace method showed a surface area of ~19 m^2g^{-1}. Comparing this initial data with g-PCN, shows a similar surface area of ~11 m^2g^{-1} (Table S2, Entry 2). Extending the milling time to 90 min shows an increase to ~57 m^2g^{-1} (Table S2, Entry 3). For the g-PCN300 material, the surface area remains unchanged at 13 m^2g^{-1} (Table S2, Entry 4) with ten 1 mm zirconia balls at ~8 m^2g^{-1} (Table S2, Entry 5). The understanding of the mechanism for P- and N-doped and bridged carbons is still under considerable investigation and debate.[100, 101] However, based on the presented data, two factors seem to be the driving force for the improved reactivity of g-PCN. Firstly, the overall addition of strongly electron donating phosphorus-linkages in place of carbon or nitrogen allows for improved charged separation with the phosphorus-linked series as opposed to g-C_3N_4, as demonstrated by a reduced PL signal and extended lifetime for the g-PCN series (Figure 4b and 4c).[101, 102] Additionally, the amorphous g-PCN showed improved catalytic activity over samples showing improved crystallinity after annealing. Therefore, it can be hypothesized that defects present in g-PCN following milling and aging allow for the trapping of photoexcited charges, previously demonstrated to improve the evolution of hydrogen.[102, 103]

Conclusion

In conclusion, we presented a mechanochemistry-based approach to phosphorus-bridged triazine based carbon nitrides. A combination of experimental and theoretical analysis confirms the successfully synthesis of several layered phosphorus-linked carbon nitride structures. Periodic DFT calculations enabled the identification of a layered structural model for the materials, which was confirmed by excellent match between calculated and measured ^{31}P NMR and PXRD data.

The photocatalytic behaviour of the resulting triazine-based materials was evaluated towards the hydrogen evolution reaction and shown to feature improvement over traditional graphitic carbon nitride producing 122 μmol H_2 h^{-1} g^{-1}. The combination of computational techniques for MAS NMR prediction and PXRD comparison has shown to be an effective tool for the evaluation of heteroatom-linked triazine based materials and should be expanded upon in future works.

ACKNOWLEDGMENT

We thank the Natural Science and Engineering Research Council of Canada (NSERC) Discovery Grant, Discovery Accelerator Supplement, the McGill Sustainability Systems Initiative (MSSI), the Fonds de Recherche du Québec – Nature et Technologies (FRQNT) - Centre for Green Chemistry and Catalysis (CGCC), the Walter C. Sumner Memorial Fellowship (B. G. F.), McGill University and Université de Laval. We thank Dr. Hatem M. Titi for his assistance in the collection of BET measurements, and Dr. Thomas Auvray for the fruitful conversations regarding photocatalytic water splitting. We thank the McGill Institute for Advanced Materials and the Mining and Materials Engineering Department at McGill University for the use of their X-ray photoelectron spectroscopy (XPS) instrument and associated Avantage processing software. This research was enabled in part by support provided by Calcul Québec (https:// www.calculquebec.ca) and Compute Canada (https://www.computecanada.ca).

† B.G.F and G.D. contributed equally to this work.

REFERENCES

1. Häussinger, P.; Lohmüller, R.; Watson, A. M., Hydrogen, 2. Production. In *Ullmann's Encyclopedia of Industrial Chemistry*, John Wiley & Sons, Ltd: 2011; Vol. 18, pp 249-307.
2. Kuang, M.; Han, P.; Wang, Q.; Li, J.; Zheng, G., CuCo Hybrid Oxides as Bifunctional Electrocatalyst for Efficient Water Splitting. *Adv. Funct. Mater.* **2016,** *26* (46), 8555-8561.
3. Yang, Y.; Niu, S.; Han, D.; Liu, T.; Wang, G.; Li, Y., Progress in Developing Metal Oxide Nanomaterials for Photoelectrochemical Water Splitting. *Adv. Eng. Mater.* **2017,** *7* (19), 1700555.
4. Hao, S.; Chen, L.; Yu, C.; Yang, B.; Li, Z.; Hou, Y.; Lei, L.; Zhang, X., NiCoMo Hydroxide Nanosheet Arrays Synthesized via Chloride Corrosion for Overall Water Splitting. *ACS Energy Lett.* **2019,** *4* (4), 952-959.
5. Wang, Y.; Yan, D.; El Hankari, S.; Zou, Y.; Wang, S., Recent Progress on Layered Double Hydroxides and Their Derivatives for Electrocatalytic Water Splitting. *Adv. Sci.* **2018,** *5* (8), 1800064.
6. Ju, L.; Dai, Y.; Wei, W.; Li, M.; Liang, Y.; Huang, B., One-dimensional cadmium sulphide nanotubes for photocatalytic water splitting. *Phys. Chem. Chem. Phys.* **2018,** *20* (3), 1904-1913.
7. Shankar, A.; Elakkiya, R.; Maduraiveeran, G., Self-supported fabrication and electrochemical water splitting study of transition-metal sulphide nanostructured electrodes. *New J. Chem.* **2020,** *44* (13), 5071-5078.
8. Guo, R.; Lai, X.; Huang, J.; Du, X.; Yan, Y.; Sun, Y.; Zou, G.; Xiong, J., Phosphate-Based Electrocatalysts for Water Splitting: Recent Progress. *ChemElectroChem* **2018,** *5* (24), 3822-3834.
9. Cao, S.; Wang, C. J.; Fu, W. F.; Chen, Y., Metal Phosphides as Co-Catalysts for Photocatalytic and Photoelectrocatalytic Water Splitting. *ChemSusChem* **2017,** *10* (22), 4306-4323.
10. Luo, F.; Zhang, Q.; Yu, X.; Xiao, S.; Ling, Y.; Hu, H.; Guo, L.; Yang, Z.; Huang, L.; Cai, W.; Cheng, H., Palladium Phosphide as a Stable and Efficient Electrocatalyst for Overall Water Splitting. *Angew. Chem. Int. Ed.* **2018,** *57* (45), 14862-14867.
11. Yu, F.; Zhou, H.; Huang, Y.; Sun, J.; Qin, F.; Bao, J.; Goddard III, W. A.; Chen, S.; Ren, Z., High-performance bifunctional porous non-noble metal phosphide catalyst for overall water splitting. *Nat. Commun.* **2018,** *9* (1), 2551.
12. Li, X.; Masters, A. F.; Maschmeyer, T., Polymeric carbon nitride for solar hydrogen production. *Chem. Commun.* **2017,** *53* (54), 7438-7446.
13. Jiang, L.; Yuan, X.; Pan, Y.; Liang, J.; Zeng, G.; Wu, Z.; Wang, H., Doping of graphitic carbon nitride for photocatalysis: A reveiw. *Appl. Catal. B* **2017,** *217*, 388-406.
14. Melissen, S.; Le Bahers, T.; Sautet, P.; Steinmann, S. N., What does graphitic carbon nitride really look like? *Phys. Chem. Chem. Phys.* **2021,** *23* (4), 2853-2859.
15. Zhang, H.; Yu, A., Photophysics and Photocatalysis of Carbon Nitride Synthesized at Different Temperatures. *J. Phys. Chem. C* **2014,** *118* (22), 11628-11635.
16. Godin, R.; Wang, Y.; Zwijnenburg, M. A.; Tang, J.; Durrant, J. R., Time-Resolved Spectroscopic Investigation of Charge Trapping in Carbon Nitrides Photocatalysts for Hydrogen Generation. *J. Am. Chem. Soc.* **2017,** *139* (14), 5216-5224.

17. Li, X.; Melissen, S. T. A. G.; Le Bahers, T.; Sautet, P.; Masters, A. F.; Steinmann, S. N.; Maschmeyer, T., Shining Light on Carbon Nitrides: Leveraging Temperature To Understand Optical Gap Variations. *Chem. Mater.* **2018,** *30* (13), 4253-4262.
18. Zhang, J.-W.; Gong, S.; Mahmood, N.; Pan, L.; Zhang, X.; Zou, J.-J., Oxygen-doped nanoporous carbon nitride via water-based homogeneous supramolecular assembly for photocatalytic hydrogen evolution. *Appl. Catal. B* **2018,** *221*, 9-16.
19. Chen, H.; Yao, J.; Qiu, P.; Xu, C.; Jiang, F.; Wang, X., Facile surfactant assistant synthesis of porous oxygen-doped graphitic carbon nitride nanosheets with enhanced visible light photocatalytic activity. *Mater. Res. Bull.* **2017,** *91*, 42-48.
20. Fan, Q.; Liu, J.; Yu, Y.; Zuo, S.; Li, B., A simple fabrication for sulfur doped graphitic carbon nitride porous rods with excellent photocatalytic activity degrading RhB dye. *Appl. Surf. Sci.* **2017,** *391*, 360-368.
21. Feng, L.-L.; Zou, Y.; Li, C.; Gao, S.; Zhou, L.-J.; Sun, Q.; Fan, M.; Wang, H.; Wang, D.; Li, G.-D.; Zou, X., Nanoporous sulfur-doped graphitic carbon nitride microrods: A durable catalyst for visible-light-driven H_2 evolution. *Int. J. Hydrogen Energy* **2014,** *39* (28), 15373-15379.
22. Hu, S.; Ma, L.; You, J.; Li, F.; Fan, Z.; Wang, F.; Liu, D.; Gui, J., A simple and efficient method to prepare a phosphorus modified g-C_3N_4 visible light photocatalyst. *RSC Adv.* **2014,** *4* (41), 21657-21663.
23. Liu, B.; Ye, L.; Wang, R.; Yang, J.; Zhang, Y.; Guan, R.; Tian, L.; Chen, X., Phosphorus-Doped Graphitic Carbon Nitride Nanotubes with Amino-rich Surface for Efficient CO_2 Capture, Enhanced Photocatalytic Activity, and Product Selectivity. *ACS Appl. Mater. Interfaces* **2018,** *10* (4), 4001-4009.
24. Wang, X.; Maeda, K.; Thomas, A.; Takanabe, K.; Xin, G.; Carlsson, J. M.; Domen, K.; Antonietti, M., A metal-free polymeric photocatalyst for hydrogen production from water under visible light. *Nat. Mater.* **2009,** *8* (1), 76-80.
25. Zhang, Y.; Mori, T.; Ye, J.; Antonietti, M., Phosphorus-doped carbon nitride solid: enhanced electrical conductivity and photocurrent generation. *J. Am. Chem. Soc.* **2010,** *132* (18), 6294-5.
26. Guo, S.; Deng, Z.; Li, M.; Jiang, B.; Tian, C.; Pan, Q.; Fu, H., Phosphorus-Doped Carbon Nitride Tubes with a Layered Micro-nanostructure for Enhanced Visible-Light Photocatalytic Hydrogen Evolution. *Angew. Chem. Int. Ed.* **2016,** *55* (5), 1830-4.
27. Zhu, Y. P.; Ren, T. Z.; Yuan, Z. Y., Mesoporous Phosphorus-Doped g-C_3N_4 Nanostructured Flowers with Superior Photocatalytic Hydrogen Evolution Performance. *ACS Appl. Mater. Interfaces* **2015,** *7* (30), 16850-6.
28. Lin, X.; Peng, P.; Guo, J.; Xiang, Z., Reaction milling for scalable synthesis of N, P-codoped covalent organic polymers for metal-free bifunctional electrocatalysts. *Chem. Eng. J.* **2019,** *358*, 427-434.
29. Ma, T. Y.; Ran, J.; Dai, S.; Jaroniec, M.; Qiao, S. Z., Phosphorus-doped graphitic carbon nitrides grown in situ on carbon-fiber paper: flexible and reversible oxygen electrodes. *Angew. Chem. Int. Ed.* **2015,** *54* (15), 4646-50.
30. Chai, B.; Yan, J.; Wang, C.; Ren, Z.; Zhu, Y., Enhanced visible light photocatalytic degradation of Rhodamine B over phosphorus doped graphitic carbon nitride. *Appl. Surf. Sci.* **2017,** *391*, 376-383.
31. Lv, H.; Zhao, X.; Niu, H.; He, S.; Tang, Z.; Wu, F.; Giesy, J. P., Ball milling synthesis of covalent organic framework as a highly active photocatalyst for degradation of organic contaminants. *J. Hazard. Mater.* **2019,** *369*, 494-502.

32. Zhang, L.; Chen, X.; Guan, J.; Jiang, Y.; Hou, T.; Mu, X., Facile synthesis of phosphorus doped graphitic carbon nitride polymers with enhanced visible-light photocatalytic activity. *Mater. Res. Bull.* **2013,** *48* (9), 3485-3491.
33. Chaloux, B. L.; Yonke, B. L.; Purdy, A. P.; Yesinowski, J. P.; Glaser, E. R.; Epshteyn, A., $P(CN)_3$ Precursor for Carbon Phosphonitride Extended Solids. *Chem. Mater.* **2015,** *27* (13), 4507-4510.
34. Wang, Q.; Gou, H.; Zhu, L.; Huang, H.-T.; Biswas, A.; Chaloux, B. L.; Epshteyn, A.; Yesinowski, J. P.; Liu, Z.; Cody, G.; Ma, M.; Zhao, Z.; Fei, Y.; Prescher, C.; Greenberg, E.; Prakapenka, V. B.; Strobel, T. A., Modifying Carbon Nitride through Extreme Phosphorus Substitution. *ACS Mater. Lett.* **2019,** *1* (1), 14-19.
35. Zou, J.; Yu, Y.; Qiao, K.; Wu, S.; Yan, W.; Cheng, S.; Jiang, N.; Wang, J., Microwave synthesis of phosphorus-doped graphitic carbon nitride nanosheets with enhanced electrochemiluminescence signals. *J. Mater. Sci.* **2020,** *55* (28), 13618-13633.
36. Crawford, D. E.; Miskimmin, C. K. G.; Albadarin, A. B.; Walker, G.; James, S. L., Organic synthesis by Twin Screw Extrusion (TSE): continuous, scalable and solvent-free. *Green Chem.* **2017,** *19* (6), 1507-1518.
37. Crawford, D. E.; Wright, L. A.; James, S. L.; Abbott, A. P., Efficient continuous synthesis of high purity deep eutectic solvents by twin screw extrusion. *Chem. Commun.* **2016,** *52* (22), 4215-8.
38. Daurio, D.; Nagapudi, K.; Li, L.; Quan, P.; Nunez, F. A., Application of twin screw extrusion to the manufacture of cocrystals: scale-up of AMG 517-sorbic acid cocrystal production. *Faraday Discuss.* **2014,** *170*, 235-49.
39. Egleston, B. D.; Brand, M. C.; Greenwell, F.; Briggs, M. E.; James, S. L.; Cooper, A. I.; Crawford, D. E.; Greenaway, R. L., Continuous and scalable synthesis of a porous organic cage by twin screw extrusion (TSE). *Chem. Sci.* **2020,** *11* (25), 6582-6589.
40. James, S. L.; Adams, C. J.; Bolm, C.; Braga, D.; Collier, P.; Friscic, T.; Grepioni, F.; Harris, K. D.; Hyett, G.; Jones, W.; Krebs, A.; Mack, J.; Maini, L.; Orpen, A. G.; Parkin, I. P.; Shearouse, W. C.; Steed, J. W.; Waddell, D. C., Mechanochemistry: opportunities for new and cleaner synthesis. *Chem. Soc. Rev.* **2012,** *41* (1), 413-47.
41. Do, J. L.; Friscic, T., Mechanochemistry: A Force of Synthesis. *ACS Cent. Sci.* **2017,** *3* (1), 13-19.
42. Tan, D.; Friščić, T., Mechanochemistry for Organic Chemists: An Update. *Eur. J. Org. Chem.* **2018,** *2018* (1), 18-33.
43. Wang, G. W., Mechanochemical organic synthesis. *Chem. Soc. Rev.* **2013,** *42* (18), 7668-700.
44. Wang, G. W., Fullerene Mechanochemistry: Serendipitous Discovery of Dumb-Bell-Shaped C120 and Beyond. *Chin. J. Chem.* **2021,** *39* (7), 1797-1803.
45. Do, J. L.; Tan, D.; Friscic, T., Oxidative Mechanochemistry: Direct, Room-Temperature, Solvent-Free Conversion of Palladium and Gold Metals into Soluble Salts and Coordination Complexes. *Angew. Chem. Int. Ed.* **2018,** *57* (10), 2667-2671.
46. Hernández, J. G.; Butler, I. S.; Friščić, T., Multi-step and multi-component organometallic synthesis in one pot using orthogonal mechanochemical reactions. *Chem. Sci.* **2014,** *5* (9), 3576-3582.
47. Koby, R. F.; Doerr, A. M.; Rightmire, N. R.; Schley, N. D.; Long, B. K.; Hanusa, T. P., An η^3 -Bound Allyl Ligand on Magnesium in a Mechanochemically Generated Mg/K Allyl Complex. *Angew. Chem. Int. Ed.* **2020,** *59* (24), 9542-9548.

48. Koby, R. F.; Hanusa, T. P.; Schley, N. D., Mechanochemically Driven Transformations in Organotin Chemistry: Stereochemical Rearrangement, Redox Behavior, and Dispersion-Stabilized Complexes. *J. Am. Chem. Soc.* **2018,** *140* (46), 15934-15942.
49. Tan, D.; Garcia, F., Main group mechanochemistry: from curiosity to established protocols. *Chem. Soc. Rev.* **2019,** *48* (8), 2274-2292.
50. Crawford, D.; Casaban, J.; Haydon, R.; Giri, N.; McNally, T.; James, S. L., Synthesis by extrusion: continuous, large-scale preparation of MOFs using little or no solvent. *Chem. Sci.* **2015,** *6* (3), 1645-1649.
51. Lv, D.; Chen, Y.; Li, Y.; Shi, R.; Wu, H.; Sun, X.; Xiao, J.; Xi, H.; Xia, Q.; Li, Z., Efficient Mechanochemical Synthesis of MOF-5 for Linear Alkanes Adsorption. *J. Chem. Eng. Data* **2017,** *62* (7), 2030-2036.
52. Beldon, P. J.; Fabian, L.; Stein, R. S.; Thirumurugan, A.; Cheetham, A. K.; Friscic, T., Rapid room-temperature synthesis of zeolitic imidazolate frameworks by using mechanochemistry. *Angew. Chem. Int. Ed. Engl.* **2010,** *49* (50), 9640-3.
53. Ashlin, M.; Hobbs, C. E., Post-Polymerization Thiol Substitutions Facilitated by Mechanochemistry. *Macromol. Chem. Phys.* **2019,** *220* (21).
54. Fiss, B. G.; Hatherly, L.; Stein, R. S.; Friščić, T.; Moores, A., Mechanochemical Phosphorylation of Polymers and Synthesis of Flame-Retardant Cellulose Nanocrystals. *ACS Sustainable Chem. Eng.* **2019,** *7* (8), 7951-7959.
55. Malca, M. Y.; Ferko, P. O.; Friscic, T.; Moores, A., Solid-state mechanochemical ω-functionalization of poly(ethylene glycol). *Beilstein J. Org. Chem.* **2017,** *13* (2004), 1963-1968.
56. Di Nardo, T.; Hadad, C.; Nguyen Van Nhien, A.; Moores, A., Synthesis of high molecular weight chitosan from chitin by mechanochemistry and aging. *Green Chem.* **2019,** *21* (12), 3276-3285.
57. Arhangelskis, M.; Bucar, D. K.; Bordignon, S.; Chierotti, M. R.; Stratford, S. A.; Voinovich, D.; Jones, W.; Hasa, D., Mechanochemical reactivity inhibited, prohibited and reversed by liquid additives: examples from crystal-form screens. *Chem. Sci.* **2021,** *12* (9), 3264-3269.
58. Friščić, T.; Childs, S. L.; Rizvi, S. A.; Jones, W., The role of solvent in mechanochemical and sonochemical cocrystal formation: a solubility-based approach for predicting cocrystallisation outcome. *CrystEngComm* **2009,** *11* (3), 418-426.
59. Amrute, A. P.; De Bellis, J.; Felderhoff, M.; Schuth, F., Mechanochemical Synthesis of Catalytic Materials. *Chem. Euro. J.* **2021,** *27* (23), 6819-6847.
60. Xu, C.; De, S.; Balu, A. M.; Ojeda, M.; Luque, R., Mechanochemical synthesis of advanced nanomaterials for catalytic applications. *Chem. Commun.* **2015,** *51* (31), 6698-713.
61. Malca, M. Y.; Bao, H.; Bastaille, T.; Saadé, N. K.; Kinsella, J. M.; Friščić, T.; Moores, A., Mechanically Activated Solvent-Free Assembly of Ultrasmall Bi_2S_3 Nanoparticles: A Novel, Simple, and Sustainable Means To Access Chalcogenide Nanoparticles. *Chem. Mater.* **2017,** *29* (18), 7766-7773.
62. Rak, M. J.; Friscic, T.; Moores, A., Mechanochemical synthesis of Au, Pd, Ru and Re nanoparticles with lignin as a bio-based reducing agent and stabilizing matrix. *Faraday Discuss.* **2014,** *170*, 155-67.
63. Rak, M. J.; Saadé, N. K.; Friščić, T.; Moores, A., Mechanosynthesis of ultra-small monodisperse amine-stabilized gold nanoparticles with controllable size. *Green Chem.* **2014,** *16* (1), 86-89.

64. Rakhimov, R. R.; Jackson, E. M.; Hwang, J. S.; Prokof'ev, A. I.; Alexandrov, I. A.; Karmilov, A. Y.; Aleksandrov, A. I., Mechanochemical synthesis of Co, Ni, Fe nanoparticles in polymer matrices. *J. Appl. Phys.* **2004,** *95* (11), 7133-7135.
65. Cheng, Z.; Fang, W.; Zhao, T.; Fang, S.; Bi, J.; Liang, S.; Li, L.; Yu, Y.; Wu, L., Efficient Visible-Light-Driven Photocatalytic Hydrogen Evolution on Phosphorus-Doped Covalent Triazine-Based Frameworks. *ACS Appl. Mater. Interfaces* **2018,** *10* (48), 41415-41421.
66. Liang, X.; Tian, N.; Zhou, Z.; Sun, S., N, P Dual-Doped Porous Carbon Nanosheets for High-Efficiency CO_2 Electroreduction. *ACS Sustainable Chem. Eng.* **2022,** *10* (5), 1880-1887.
67. Zhao, Z.; Xie, C.; Cui, H.; Wang, Q.; Shu, Z.; Zhou, J.; Li, T., Scalable one-pot synthesis of phosphorus-doped g-C_3N_4 nanosheets for enhanced visible-light photocatalytic hydrogen evolution. *Diam. Relat. Mater.* **2020,** *104*, 107734.
68. Le Corre, G.; Grutzmacher, H., Simple conversion of trisodium phosphide, Na_3P, into silyl- and cyanophosphides and the structure of a terminal silver phosphide. *Dalton Trans.* **2022,** *51* (9), 3497-3501.
69. Fiss, B. G.; Vu, N.-N.; Douglas, G.; Do, T.-O.; Friščić, T.; Moores, A., Solvent-Free Mechanochemical Synthesis of Ultrasmall Nickel Phosphide Nanoparticles and Their Application as a Catalyst for the Hydrogen Evolution Reaction (HER). *ACS Sustainable Chem. Eng.* **2020,** *8* (32), 12014-12024.
70. Fiss, B. G.; Richard, A. J.; Douglas, G.; Kojic, M.; Friscic, T.; Moores, A., Mechanochemical methods for the transfer of electrons and exchange of ions: inorganic reactivity from nanoparticles to organometallics. *Chem. Soc. Rev.* **2021,** *50* (14), 8279-8318.
71. Takacs, L., Self-sustaining reactions induced by ball milling: An overview. *Int. J. Self-Propag. High-Temp. Synth.* **2010,** *18* (4), 276-282.
72. Takacs, L., The historical development of mechanochemistry. *Chem. Soc. Rev.* **2013,** *42* (18), 7649-59.
73. Takacs, L.; Mandal, S. K., Preparation of some metal phosphides by ball milling. *Mater. Sci. Eng. A* **2001,** *304-306* (1-2), 429-433.
74. Casco, M. E.; Kirchhoff, S.; Leistenschneider, D.; Rauche, M.; Brunner, E.; Borchardt, L., Mechanochemical synthesis of N-doped porous carbon at room temperature. *Nanoscale* **2019,** *11* (11), 4712-4718.
75. Troschke, E.; Gratz, S.; Lubken, T.; Borchardt, L., Mechanochemical Friedel-Crafts Alkylation-A Sustainable Pathway Towards Porous Organic Polymers. *Angew. Chem. Int. Ed.* **2017,** *56* (24), 6859-6863.
76. Cliffe, M. J.; Mottillo, C.; Stein, R. S.; Bučar, D.-K.; Friščić, T., Accelerated aging: a low energy, solvent-free alternative to solvothermal and mechanochemical synthesis of metal–organic materials. *Chem. Sci.* **2012,** *3* (8), 2495-2500.
77. Huskić, I.; Lennox, C. B.; Friščić, T., Accelerated ageing reactions: towards simpler, solvent-free, low energy chemistry. *Green Chem.* **2020,** *22* (18), 5881-5901.
78. de Oliveira, P. F. M.; Michalchuk, A. A. L.; Buzanich, A. G.; Bienert, R.; Torresi, R. M.; Camargo, P. H. C.; Emmerling, F., Tandem X-ray absorption spectroscopy and scattering for in situ time-resolved monitoring of gold nanoparticle mechanosynthesis. *Chem. Commun.* **2020,** *56* (71), 10329-10332.
79. Yan, S. C.; Li, Z. S.; Zou, Z. G., Photodegradation performance of g-C_3N_4 fabricated by directly heating melamine. *Langmuir* **2009,** *25* (17), 10397-401.
80. Schneidermann, C.; Kensy, C.; Otto, P.; Oswald, S.; Giebeler, L.; Leistenschneider, D.; Gratz, S.; Dorfler, S.; Kaskel, S.; Borchardt, L., Nitrogen-Doped Biomass-Derived Carbon

Formed by Mechanochemical Synthesis for Lithium-Sulfur Batteries. *ChemSusChem* **2019,** *12* (1), 310-319.
81. Ma, J.; Jin, D.; Yang, X.; Sun, S.; Zhou, J.; Sun, R., Phosphorus-doped carbon nitride with grafted sulfonic acid groups for efficient photocatalytic synthesis of xylonic acid. *Green Chem.* **2021,** *23* (11), 4150-4160.
82. Fang, X.-X.; Ma, L.-B.; Liang, K.; Zhao, S.-J.; Jiang, Y.-F.; Ling, C.; Zhao, T.; Cheang, T.-Y.; Xu, A.-W., The doping of phosphorus atoms into graphitic carbon nitride for highly enhanced photocatalytic hydrogen evolution. *J. Mater. Chem. A* **2019,** *7* (18), 11506-11512.
83. Lin, L.; Wang, C.; Ren, W.; Ou, H.; Zhang, Y.; Wang, X., Photocatalytic overall water splitting by conjugated semiconductors with crystalline poly(triazine imide) frameworks. *Chem. Sci.* **2017,** *8* (8), 5506-5511.
84. Alwin, E.; Koci, K.; Wojcieszak, R.; Zielinski, M.; Edelmannova, M.; Pietrowski, M., Influence of High Temperature Synthesis on the Structure of Graphitic Carbon Nitride and Its Hydrogen Generation Ability. *Materials* **2020,** *13* (12), 2756.
85. Dutta, A.; Reid, C.; Heinrich, H., Simulation of Incoherent Scattering in High-Angle Annular Dark-Field Scanning Electron Microscopy. *Microsc. Microanal.* **2013,** *19* (S2), 852-853.
86. Van den Broek, W.; Rosenauer, A.; Goris, B.; Martinez, G. T.; Bals, S.; Van Aert, S.; Van Dyck, D., Correction of non-linear thickness effects in HAADF STEM electron tomography. *Ultramicroscopy* **2012,** *116*, 8-12.
87. Mohamed, N. A.; Safaei, J.; Ismail, A. F.; Jailani, M. F. A. M.; Khalid, M. N.; Noh, M. F. M.; Aadenan, A.; Nasir, S. N. S.; Sagu, J. S.; Teridi, M. A. M., The influences of post-annealing temperatures on fabrication graphitic carbon nitride, (g-C_3N_4) thin film. *Appl. Surf. Sci.* **2019,** *489*, 92-100.
88. Ma, X.; Lv, Y.; Xu, J.; Liu, Y.; Zhang, R.; Zhu, Y., A Strategy of Enhancing the Photoactivity of g-C_3N_4 via Doping of Nonmetal Elements: A First-Principles Study. *J. Phys. Chem. C* **2012,** *116* (44), 23485-23493.
89. Pu, X.-L.; Yang, X.-C.; Liang, S.-S.; Wang, W.; Zhao, J.-T.; Zhang, Z.-J., Self-assembly of a g-C_3N_4-based 3D aerogel induced by N-modified carbon dots for enhanced photocatalytic hydrogen production. *J. Mater. Chem. A* **2021,** *9* (39), 22373-22379.
90. Samanta, S.; Battula, V. R.; Sardana, N.; Kailasam, K., Solar driven photocatalytic hydrogen evolution using graphitic-carbon nitride/NSGQDs heterostructures. *Appl. Surf. Sci.* **2021,** *563*, 150409-150417.
91. Vu, N. N.; Nguyen, C. C.; Kaliaguine, S.; Do, T. O., Synthesis of g-C_3N_4 Nanosheets by Using a Highly Condensed Lamellar Crystalline Melamine-Cyanuric Acid Supramolecular Complex for Enhanced Solar Hydrogen Generation. *ChemSusChem* **2019,** *12* (1), 291-302.
92. Vu, N.-N.; Kaliaguine, S.; Do, T.-O., Selective Fragmentation through C–N Bond Cleavage of Carbon Nitride Framework for Enhanced Photocatalytic Hydrogen Production. *ACS Sustainable Chem. Eng.* **2019,** *8* (2), 853-863.
93. Ou-Yang, J.; Zhu, K.; Li, X.; Zhu, Y.; Song, Y.; Cui, Y., Carbon quantum dots modified oxygen doped carbon nitride nanosheets with enhanced hydrogen evolution under visible light irradiation. *J. Mol. Struct.* **2021,** *1229*, 129585.
94. Nasir, M. S.; Yang, G.; Ayub, I.; Wang, S.; Wang, L.; Wang, X.; Yan, W.; Peng, S.; Ramakarishna, S., Recent development in graphitic carbon nitride based photocatalysis for hydrogen generation. *Appl. Catal. B* **2019,** *257*, 117855.
95. Frisch, M. J.; Trucks, G. W.; Schlegel, H. B.; Scuseria, G. E.; Robb, M. A.; Cheeseman, J. R.; Scalmani, G.; Barone, V.; Petersson, G. A.; Nakatsuji, H.; Li, X.; Caricato, M.; Marenich,

A. V.; Bloino, J.; Janesko, B. G.; Gomperts, R.; Mennucci, B.; Hratchian, H. P.; Ortiz, J. V.; Izmaylov, A. F.; Sonnenberg, J. L.; Williams; Ding, F.; Lipparini, F.; Egidi, F.; Goings, J.; Peng, B.; Petrone, A.; Henderson, T.; Ranasinghe, D.; Zakrzewski, V. G.; Gao, J.; Rega, N.; Zheng, G.; Liang, W.; Hada, M.; Ehara, M.; Toyota, K.; Fukuda, R.; Hasegawa, J.; Ishida, M.; Nakajima, T.; Honda, Y.; Kitao, O.; Nakai, H.; Vreven, T.; Throssell, K.; Montgomery Jr., J. A.; Peralta, J. E.; Ogliaro, F.; Bearpark, M. J.; Heyd, J. J.; Brothers, E. N.; Kudin, K. N.; Staroverov, V. N.; Keith, T. A.; Kobayashi, R.; Normand, J.; Raghavachari, K.; Rendell, A. P.; Burant, J. C.; Iyengar, S. S.; Tomasi, J.; Cossi, M.; Millam, J. M.; Klene, M.; Adamo, C.; Cammi, R.; Ochterski, J. W.; Martin, R. L.; Morokuma, K.; Farkas, O.; Foresman, J. B.; Fox, D. J. *Gaussian 16 Rev. C.01*, Wallingford, CT, 2016.

96. Clark, S. J.; Segall, M. D.; Pickard, C. J.; Hasnip, P. J.; Probert, M. I. J.; Refson, K.; Payne, M. C., First principles methods using CASTEP. *Z. Kristallogr.* **2005,** *220* (5-6), 567-570.

97. Algara-Siller, G.; Severin, N.; Chong, S. Y.; Bjorkman, T.; Palgrave, R. G.; Laybourn, A.; Antonietti, M.; Khimyak, Y. Z.; Krasheninnikov, A. V.; Rabe, J. P.; Kaiser, U.; Cooper, A. I.; Thomas, A.; Bojdys, M. J., Triazine-based graphitic carbon nitride: a two-dimensional semiconductor. *Angew. Chem. Int. Ed.* **2014,** *53* (29), 7450-5.

98. Ardila-Fierro, K. J.; Hernandez, J. G., Sustainability Assessment of Mechanochemistry by Using the Twelve Principles of Green Chemistry. *ChemSusChem* **2021,** *14* (10), 2145-2162.

99. DeSantis, D.; Mason, J. A.; James, B. D.; Houchins, C.; Long, J. R.; Veenstra, M., Techno-economic analysis of metal–organic frameworks for hydrogen and natural gas storage. *Energy Fuels* **2017,** *31* (2), 2024-2032.

100. Hung, Y.-H.; Dutta, D.; Tseng, C.-J.; Chang, J.-K.; Bhattacharyya, A. J.; Su, C.-Y., Manipulation of Heteroatom Substitution on Nitrogen and Phosphorus Co-Doped Graphene as a High Active Catalyst for Hydrogen Evolution Reaction. *J. Phys. Chem. C* **2019,** *123* (36), 22202-22211.

101. Liu, Z.; Ai, J.; Sun, M.; Han, F.; Li, Z.; Peng, Q.; Wang, Q. D.; Liu, J.; Liu, L., Phosphorous-Doped Graphite Layers with Outstanding Electrocatalytic Activities for the Oxygen and Hydrogen Evolution Reactions in Water Electrolysis. *Adv. Funct. Mater.* **2020,** *30* (12), 1910741.

102. Starukh, H.; Praus, P., Doping of Graphitic Carbon Nitride with Non-Metal Elements and Its Applications in Photocatalysis. *Catalysts* **2020,** *10* (10), 1119-1156.

103. Zhang, Z.; Lu, L.; Lv, Z.; Chen, Y.; Jin, H.; Hou, S.; Qiu, L.; Duan, L.; Liu, J.; Dai, K., Porous carbon nitride with defect mediated interfacial oxidation for improving visible light photocatalytic hydrogen evolution. *Appl. Catal. B* **2018,** *232*, 384-390.